18th International Conference
ENGINEERING MECHANICS 2012
Svratka, Czech Republic, May 14 – 17, 2012

pp. 719–724
Paper #125

# MODELING OF MACROSCOPIC ELASTIC PROPERTIES OF ALUMINIUM FOAM

**V. Králík[*], J. Němeček[**]**

**Abstract:** *This paper is focused on the prediction of macroscopic elastic properties of highly porous aluminium foam. The material is characterized by a closed pore system with very thin pore walls and large air pores. Intrinsic material properties of cell wall constituents are assessed with nanoindentation whereas analytical homogenizations are employed for the assessment of the cell wall elastic properties. Very good agreement was found between the various analytical estimates. Two-dimensional microstructural FEM model was applied to obtain effective elastic properties of the upper material level. for which the Young's modulus reached 1.11 GPa. The value is by ~30% lower than the range of experimental values obtained from experimental compression tests. It follows from the 2-D approximation that the 2-D model underestimates the stiffness, by ~30% compared to the real case constrained in 3-D. Therefore, more appropriate 3-D model based on microCT data will be prepared in the future work.*

**Keywords:** ***metal foam, porous system, nanoindentation, micromechanical properties, homogenization.***

## 1. Introduction

Traditionally, materials are tested on large samples by macroscopic methods that can give overall (or effective) properties. Together with the development of experimental techniques in the past, microstructural and micromechanical properties have become important in the description of the material behavior since they could give answers on the origin of many macrolevel phenomena.

Aluminium foams belong to the up-to-date structural materials with high potential to many engineering applications. This highly porous material with a cellular structure is known for its attractive mechanical and physical characteristics. The application of this material is very wide. Some structural and functional applications of aluminium foams for industrial sector which covers mainly automotive, aircraft but also building industries have been reviewed e.g. by Banhart (2001).

In general, mechanical properties of metal foams are governed by two major factors: (i) cell morphology (shape, size and distribution of cells) and (ii) material properties of the cell walls (Miyoshi et al., 1998). However, measurement of mechanical properties of the cell walls is a difficult problem that cannot be solved with conventional methods due to their small dimensions, low local bearing capacity and local yielding and bending of the cell walls. These problems can be overcome using micromechanical methods, namely nanoindentation, in which the load–displacement curve is obtained in the sub-micrometer range.

In this study, micromechanical analysis of a commercially available aluminium foam Alporas® (Shinko Wire Co., Ltd) was performed. Nanoindentation technique was applied to access elastic properties of the distinct phases within the cell walls. Based on these results, overall effective elastic properties (Young's modulus) of the solid phase were evaluated by several homogenization schemes. To calculate the effective elastic properties at the whole structural level (including the air pores) microstructural FEM model was applied.

[*] Ing. Vlastimil Králík: Faculty of Civil Engineering, Department of Mechanics, Czech Technical University in Prague, Thákurova 2077/7; 166 29, Prague; CZ, e-mail: vlastimil.kralik@fsv.cvut.cz

[**] Doc. Ing. Jiří Němeček, Ph.D.: Faculty of Civil Engineering, Department of Mechanics, Czech Technical University in Prague, Thákurova 2077/7; 166 29, Prague; CZ, e-mail: jiri.nemecek@fsv.cvut.cz

## 2. Material characterization

### 2.1. Structure of Al-foam

The properties of Al-foam depend directly on the shape and structure of the cells, therefore description of its structure is very important. The Alporas foam is characterized by a hierarchical microstructure with the system of closed pores. An internal structure of the aluminum foam is shown in Fig. 1. The most important structural characteristic of a cellular solid is its relative density, $\rho / \rho_s$ (where $\rho$ is the foam density and $\rho_s$ is the density of the solid, i.e. Al). The fraction of pore space in the foam can be defined by its porosity (1- $\rho / \rho_s$) (Gibson, 1997). The porosity was detected by weighing of a sufficiently large foam sample and by taking into account the density of pure aluminum (2700 kg/m$^3$). The relative density was assessed as 0.0859 and porosity reached 0.914, i.e. 91.4%.

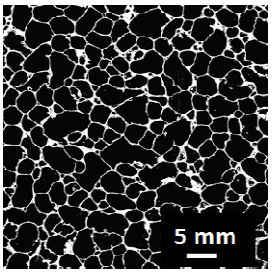


*Fig. 1. Overall view on a typical structure of aluminium foam*

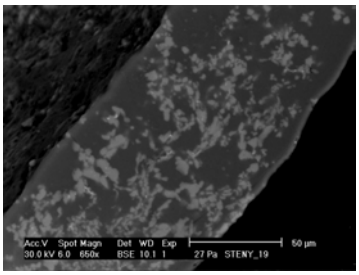

*Fig. 2. ESEM image of a cell wall*

Other important parameters for the description of the internal foam structure are both distribution of cell wall thicknesses and pore size and shape characteristics. These geometric parameters of the cell structure are crucial for the selection of the homogenization schemes and modeling mechanical performance. A high resolution optical image of the foam surface on a cross-section embedded to blackwashed gypsum was prepared. Prior to imaging the specimen was mechanically polished with fine SiC papers to receive smooth and flat surface. Size of the scanned area was 112 × 158 mm (which is sufficiently large to represent a structural level of the material).

The cell wall thickness assessed as the minimum distance between neighboring pores was evaluated using image analysis. Distribution of the cell wall thicknesses for is shown in Fig. 3. The distribution shows a significant peak, i.e. a characteristic thickness, around $L$~61 μm. The majority of cell wall thicknesses lies between 20 to 200 μm.

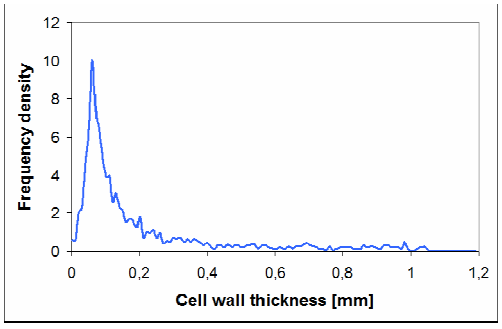


*Fig. 3 Distribution of cell wall thickness*

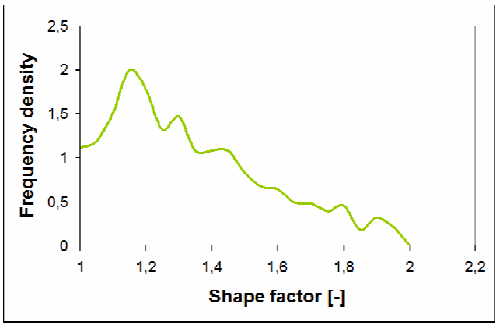


*Fig. 4 Distribution of shape factor*

A characteristic size of each pore was also estimated with the help of image analysis. Some small corrections and noise filtering in the binary image was necessary to help the algorithm automatically identify all individual pores. The pores are almost spherical or polyhedral shape due to a high foaming ratio.In the analysis, the pores were replaced by equivalent ellipses. Further, a shape factor computed as the ratio between the longer and shorter axes of the ellipse was obtained. Distribution of the values of shape factor is shown in Fig. 4. The mean value of shape factor was 1.15. This value indicates that the shape of the pores is nearly circular with a small flattening.

An equivalent pore diameter assuming circular pores was also calculated. The distribution of this equivalent pore diameters can be seen in Fig. 5. The equivalent diameters of pores are distributed over a range of 0.2 mm to 6 mm and the mean value of the equivalent diameter is 2.9 mm.

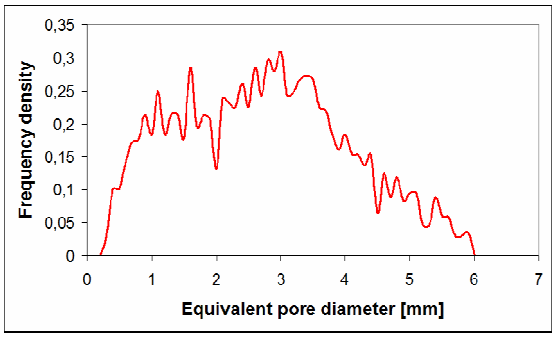


*Fig. 5 Distribution of equivalent diameter*

### 2.2. Definition of the model

At least two characteristic length scales can be distinguished for the material: the cell wall level and the foam level. Therefore, two-scale microstructural model for the prediction of macroscopic elastic properties on the whole foam level is proposed based on the utilization of nanoindentation data received on cell walls (Němeček et al., 2011; Hasan et al., 2008). The model covers:

- **Level I** (the cell wall level).

In this level, characteristic dimension of the cell wall defined by the mean midspan wall thickness is $L$~61 µm. This level consists of prevailing aluminium matrix (Al-rich area) with embedded heterogeneities in the form of Ca/Ti-rich areas (Králík et al., 2011). Distinct elastic properties of the microstructural constituents were assessed using nanoindentation at this level.

- **Level II** (the foam level).

At this level, the whole foam containing large pores with an average diameter ~2.9 mm are considered. Cell walls are considered as homogeneous having the properties that come from the Level I homogenization.

## 3. Level I homogenization

Firstly, intrinsic elastic properties of the microstructural constituents were assessed by nanoindentation at this level. Detailed description of the experimental part can be found in Němeček et al., 2011. Two-phase system (major Al-rich and minor Ca/Ti-rich phase) was assumed in the statistical deconvolution algorithm (Constantinides et al., 2006) to obtain Young's moduli and volume fractions of the two phases (Tab. 1). Poisson's ratio 0.35 was considered for both phases. Based on these results, effective elastic properties (Young's modulus) of the solid phase were evaluated by selected analytical homogenization schemes, namely Voigt and Reuss bounds, Mori-Tanaka method and self-consistent scheme (Zaoui, 2002). The homogenized elastic modulus for the cell wall is summarized in Tab. 2. Very close bounds and insignificant differences in the elastic moduli estimates by the schemes were found.

*Tab. 1: Elastic moduli and volume fractions of the two microstructural phases from deconvolution*

| Input values from nanoindentation | Mean E (GPa) | St.dev. (GPa) | Volume fraction |
|---|---|---|---|
| Al-rich zone | 61.9 | 4.6 | 0.638 |
| Ca/Ti-rich zone | 87 | 17 | 0.362 |

*Tab. 2: Effective values of Young's modulus computed by different homogenization schemes at Level I*

| Scheme | Mori-Tanaka | Self-consist. scheme | Voigt bound | Reuss bound |
|---|---|---|---|---|
| $E_{eff,\ Level\ I}$ (GPa) | 70.076 | 70.135 | 71.118 | 69.195 |

## 4. Level II homogenization

At this level, cell walls are considered as a homogeneous phase having the properties that come from the Level I homogenization. The cell walls create a matrix phase and the large air pores can be considered as inclusions in this homogenization.

At first, effective elastic properties of the Level II were estimated with the same analytical schemes used in Level I. The volume of air pores was evaluated experimentally (Section 2.1) on our samples as 91.41 %. The homogenized elastic modulus for the Level II structure is summarized in Tab. 3. It is clear from Tab. 3 that the analytical schemes show a high dispersion of results. None of the schemes used here give appropriate results compared to experiments. Nevertheless, the correct solution should lie between Voight and Reuss bounds that are, in this case, quite distant (Tab. 3). The Mori-Tanaka ends up close to the average phase value, whereas the self-consistent scheme tends to reach lower stiffness value (i.e. the air) due to the very large volume fraction of pores.

*Tab. 3: Effective values of Young's modulus computed by different analytical homogenization schemes at Level II*

| Scheme | Mori-Tanaka | Self-consist. scheme | Voigt bound | Reuss bound |
|---|---|---|---|---|
| $E_{eff,\ Level\ II}$ (GPa) | 3.1510 | 0.0012 | 6.0200 | 0.0011 |

At second, the more appropriate two dimensional microstructural FEM model was applied. The model geometry was generated from high resolution optical images of Al-foam cross-section, whose preparation is described in section 2.1. Size of the selected representative area was 60×60 mm and was rotated about both coordinate axes (axes of symmetry). Resulting area with a size of 120×120 mm was thus created to represent a higher structural level of the material. At this image, pore centroids were detected, Delaunay triangulation applied and Voronoi cells created. Then, an equivalent 2D-beam structure was generated from cell boundaries (Fig. 6). As a first estimate, uniform cross-sectional area was prescribed to all beams (~8.59 % of the total area).

The aim of the numerical analysis was to determine the effective elastic constants using the micromechanical approach in which the homogenized medium (a composite) should exhibit the same deformation behavior as the microscopically inhomogeneous sample in an average sense, In this analysis, prescribed macroscopic strain $\mathbf{E}$ is imposed on the boundaries of the RVE and microscopic strains and stresses are solved in the RVE. Volumetric averaging of microscopic stresses leads to the assessment of an average macroscopic stress and finally estimation of effective stiffness parameters.

The key issue of the computation is the size of RVE and application of boundary conditions around the domain. Since the RVE size is always smaller than an infinite body, any constraints can strongly influence the results. Application of the kinematic boundary conditions leads to the overestimation of effective stiffness and it can give an upper bound, whereas the static boundary conditions give a lower bound (Šmilauer, 2006). The best solution is usually provided by applying periodic boundary conditions to RVE which are, however, difficult to implement into commercial codes.

Nevertheless, the influence of the boundary conditions on microscopic strains and stresses in the domain decrease in distant points from the boundary. The size of our domain (120×120 mm) allowed us to solve the problem with kinematic boundary conditions. For homogenization, considerably smaller region (20×20 mm) was used. Microscopic strains and stresses were computed inside this

smaller area which was still sufficiently large to describe the material inhomogeneities and to serve as material RVE.

The whole domain (120×120 mm) was subjected to homogeneous macroscopic strain in one axial direction ($\mathbf{E}=\{1,0,0\}^T$) by imposing prescribed displacement to one domain side (Fig. 6). The test was performed using Oofem software package (Patzák et al., 2001) and microscopic strains and stresses solved in the domain. Strains and stresses (structural forces for the case of beams, respectively) inside the smaller area (20×20 mm) were averaged and used for computation of the homogenized stiffness matrix (one column in the matrix, respectively). Assuming material isotropy, the (1,1) member at the material stiffness matrix is given by:

$$L_{11} = E\frac{(1-\nu)}{(1+\nu)(1-2\nu)},$$

in which $E$ is the Young's modulus and ν Poisson's ratio, respectively. Since the Poisson's ratio of the whole foam is close to zero (as confirmed by experimental measurements) the $L_{11}$ member coincides with the Young's modulus $E$. For the tension test in x-direction (Fig.6), the homogenized Young's modulus was found to be $E_{hom}$ = 1.11 GPa.

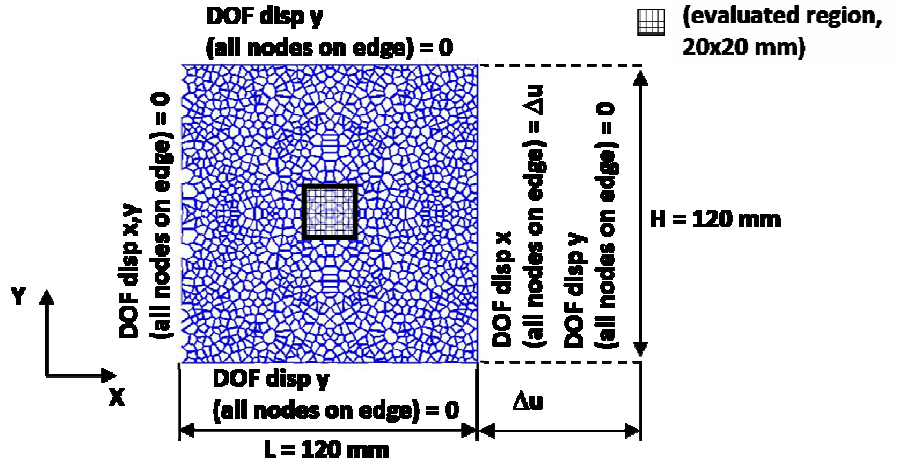


*Fig. 6. 2D-beam structure with prescribed boundary conditions.*

Such stiffness is comparable with the range of experimental values (0.4−1 GPa) reported for Alporas® e.g. by Ashby et. al. (2002). It is lower than first results obtained from our currently running experimental measurements (uniaxial compression test on 30×30×60 mm Alporas blocks) that indicate E≈1.45 GPa. The lower stiffness obtained from two-dimensional model can be explained by the lack of additional confinement appearing the three-dimensional case. Therefore, the results of the simplified 2-D model can be treated as a first estimate of the Level II material properties which need to be refined. The real confinement of a 3-D cell structure can hardly be captured in 2-D computation and leads to the necessity of the 3-D computation.

## 5. Conclusions

The microstructure of Al-foam was studied by image analysis and phase properties assessed with nanoindentation. Important parameters such as relative density (0.0859), porosity (0.914), distribution of cell wall thicknesses, distribution of equivalent pore diameters and shape factors of pores were determined. Two-scale micromechanical model was proposed for the assessment of foam effective elastic properties. Elastic parameters of cell walls (Level I) were obtained from statistical nanoindentation results from which one dominant and one minor mechanical phase were separated by the deconvolution algorithm. Application of analytical homogenization schemes showed very similar results of effective cell wall elastic properties ($E_{Level\text{-}I} \approx 70$ GPa). This value together with corresponding volume fraction of cell walls and large pores were used in micromechanical up-scaling to the upper level (Level II). Effective elastic properties of Level II were estimated with the same analytical schemes used in Level I. However, the analytical methods do not give satisfactory results in

this case. Therefore more appropriate two dimensional microstructural FEM model was applied. Homogenized Young's modulus reached 1.11 GPa. The estimated value was lower by 30% compared to experimental results (1.45 GPa). It is primarily due to the three dimensional effects (cell shape, additional confinement) that cannot be captured in the two dimensional model. Therefore, further development of the numerical model (influence of beam stiffness variations, size of RVE, extension to 3-D) and extending an experimental program is planned in the near future.

**Acknowledgement**

Support of the Czech Science Foundation (GAČR P105/12/0824) and the Grant Agency of the Czech Technical University in Prague (SGS12/116/OHK1/2T/11) is gratefully acknowledged.

**References**

Ashby M. F., Evans A., Fleck N. A., Gibson L. J., Hutchinson J. W., Wadley H. N. (2002) Metal foams: a design guide, Materials & Design, 23, 1.

Banhart J. (2001) Manufacture, characterisation and application of cellular metals and metal foams. Progress in Materials Science, 46, 6, pp.559-632.

Constantinides G., Chandran K.R., Ulm F.-J. & Vliet K.V. (2006) Grid indentation analysis of composite microstructure and mechanics: Principles of validation, Mat. Sci. and Eng., 430, 1-2, pp.189-202.

Gibson L. J., Ashby M. F. (1997) *Cellular solids – Structure and properties*. Cambridge University Press, Cambridge.

Hasan M.A., Kim A. & Lee H.-J. (2008) Measuring the cell wall mechanical properties of Al-alloy foams using the nanoindentation method, Composite Structures, 83, 2, pp.180-188.

Miyoshi T., Itoh M., Akiyama S. & Kitahara A. (1998) Aluminium foam, "ALPORAS": The production process, properties and application, Mat. Res. Soc. Symp. Proc., 521, pp.133-137.

Němeček J., Králík V., Vondřejc J., Němečková J. (2011) Identification of micromechanical properties on metal foams using nanoindentation, in: *Proceedings of the Thirteenth International Conference on Civil, Structural and Environmental Engineering Computing* (Edinburgh: Civil-Comp. Press), pp. 1-12.

Patzák B., Bittnar Z.(2001) Design of object oriented finite element code, Advances in Engineering Software, 32, 10-11, pp. 759-767.

Šmilauer V. (2006) Elastic properties of hydrating cement paste determined from hydration models, Doctoral thesis, Czech Technical University in Prague.

Zaoui A. (2002) Continuum Micromechanics: Survey, Journal of Engineering Mechanics, 128, 8, pp.808-816.